



1 Amplification of light absorption of black carbon associated with air 2 pollution

3 Yuxuan Zhang^{1,2}, Qiang Zhang¹, Yafang Cheng^{3,2}, Hang Su^{3,2}, Haiyan Li⁴, Meng Li^{1,2}, Xin Zhang¹,
4 Aijun Ding⁵, and Kebin He⁴

5 ¹Ministry of Education Key Laboratory for Earth System Modeling, Department of Earth System Science, Tsinghua
6 University, Beijing 100084, China

7 ²Multiphase Chemistry Department, Max Planck Institute for Chemistry, Mainz 55020, Germany

8 ³Institute for Environmental and Climate Research, Jinan University, Guangzhou 510630, China

9 ⁴State Key Joint Laboratory of Environment Simulation and Pollution Control, School of Environment, Tsinghua University,
10 Beijing 100084, China

11 ⁵Institute for Climate and Global Change Research, School of Atmospheric Sciences, Nanjing University, Nanjing, China

12 *Correspondence to:* Qiang Zhang (qiangzhang@tsinghua.edu.cn)

13 **Abstract.** The impacts of black carbon (BC) aerosols on air quality, boundary layer dynamic and climate depend not only on
14 the BC mass concentration but also on the light absorption capability of BC. It well known that the light absorption
15 capability of BC depends on the amount of coating materials (namely other species on BC by condensation and coagulation).
16 However, the difference of light absorption capability of ambient BC-containing particles under different air pollution
17 conditions (e.g., the air clean and polluted conditions) remains unclear due to the complex aging process of BC in the
18 atmosphere. In this work, we investigated the evolution of light absorption capability for BC-containing particles with
19 changing pollution levels in urban Beijing, China. During the campaign period (17 to 30 November 2014), with the growth
20 of PM₁ concentration from $\sim 10 \mu\text{g m}^{-3}$ to $\sim 230 \mu\text{g m}^{-3}$, we found that the aging degree and light absorption capability of BC-
21 containing particles with refractory BC cores of $\sim 75\text{-}200 \text{ nm}$ increased by 26-73% and 13-44% respectively, indicating
22 stronger light absorption capability of BC-containing particles under more polluted conditions due to more coating materials
23 on the BC surface. By using effective emission intensity (EEI) model, we further found that aging during the regional
24 transport plays an important role in the difference among the light absorption capability of BC-containing particles under
25 different air pollution levels. During the pollution episode, $\sim 63\%$ of the BC over Beijing originated from regional sources
26 outside of Beijing. These regionally sourced BC-containing particles were characterized by more coating materials on BC
27 surface due to accelerated aging process within more polluted air, which contributed $\sim 78\%$ of the increase in light absorption
28 capability of BC observed in Beijing during the polluted period (PM₁ of $\sim 230 \mu\text{g m}^{-3}$) comparing to that in the clean period



1 (PM₁ of ~10 μg m⁻³). Due to the increase of light absorption capability of BC associated with air pollution, the direct
2 radiative forcing of BC was estimated to be increased by ~20% based on a simple radiation transfer model. Our work
3 identified an amplification of light absorption and direct radiative forcing under more air polluted environment due to more
4 coating pollutants on BC. The air pollution control measures may, on the other hand, break the amplification effect by
5 reducing both emissions of BC and the coating materials and achieve co-benefits of both air quality and climate.

6 **1 Introduction**

7 Black carbon (BC) is an important aerosol component that absorbs visible sunlight and contributes to heating of the
8 atmosphere (Bond and Bergstrom, 2006; Gustafsson and Ramanathan, 2016; Menon et al., 2002). Atmospheric BC can
9 impact climate through radiative effects, which are strongly associated with the optical properties of BC, especially the light
10 absorption (Cheng et al., 2006; Jacobson, 2000; Lesins et al., 2002; Ramanathan and Carmichael, 2008). Estimating the
11 climate effects of BC is one of the major challenges in climate change research, partly due to large uncertainties in the light
12 absorption capability of BC under ambient conditions (Cappa et al. 2012; Liu et al. 2015; Liu et al. 2017; Gustafsson and
13 Ramanathan, 2016). The light absorption capability of atmospheric BC is complex and poorly quantified, and it changes with
14 the morphology, density and aging degree of the BC particles (Moffet et al., 2009; Zhang et al., 2008; Zhang et al., 2016).
15 Previous studies showed a broad range of absorption enhancements of BC during the atmospheric aging process, ranging
16 from 1.05 to 3.50 (Jacobson, 2001; Peng et al., 2016; Schnaiter et al., 2005). To date, conflicts remain between model- and
17 observation-based studies of the light absorption capability of atmospheric BC-containing particles (Cappa et al., 2012;
18 Jacobson, 2001; Liu et al. 2015; Liu et al. 2017).

19 The light absorption capability of BC-containing particles depends strongly on the particle mixing state (Liu et al. 2015;
20 Liu et al. 2017), i.e., the degree of internal mixing between BC and other particle species (i.e., non-BC components) by the
21 atmospheric aging process (i.e., condensation, coagulation and heterogeneous oxidation). The non-BC species (i.e., coating
22 materials) on the surface of BC can enhance BC light absorption via the lens effect (Bond et al., 2006; Fuller et al., 1999;
23 Jacobson, 2001; Lack and Cappa, 2010). More coating materials results in stronger light absorption capability for the BC-
24 containing particles. The coating materials on the BC surface are controlled by secondary processes (e.g., photochemical
25 production) (Metcalf et al., 2013).

26 The production of secondary aerosols in the atmosphere varies significantly with pollution levels (Cheng, 2008; Zheng et
27 al., 2016; Yang et al., 2015), indicating that BC-containing particles most likely exert different light absorption capability
28 values under different pollution levels. Compared with air clean conditions, polluted periods feature more secondary
29 aerosols, especially secondary inorganic species such as sulfate (Guo et al., 2014; Sun et al., 2014; Zheng et al., 2015). The
30 increase in secondary aerosols with increasing air pollution levels affects the amount of coating materials on the BC surface,
31 resulting in changes in the light absorption capability of the ambient BC-containing particles. Recent quasi-atmospheric
32 measurements have revealed that a clear distinction in the light absorption capability of BC-containing particles exists



1 between urban cities in developed and developing countries (Peng et al., 2016), and this difference is likely due to the
2 differences in air pollution levels.

3 To date, whether and how the aging degree and light absorption capability of BC-containing particles will change with
4 air pollution development is still unclear. Although the enhancement of BC light absorption due to coating materials on BC
5 surface has already been intensively investigated (Moffet et al., 2009; Schnaiter et al., 2005; Shiraiwa et al., 2010; Zhang et
6 al., 2016), there are few studies on the evolution of the light absorption capability of BC-containing particles with changing
7 air pollution levels. The variation in the light absorption capability of BC associated with air pollution can lead to different
8 effects of BC aerosols on air quality and climate under different pollution levels. To improve the evaluation of BC-related
9 effects on air quality and climate, some models have considered BC internally mixed with other species (namely coating
10 materials on BC surface), which can affect the light absorption capability of BC. However, the difference of coating
11 materials on BC under different air pollution conditions remains unclear.

12 In this work, we conducted an intensive field measurement campaign in urban Beijing, China, to investigate the
13 difference of the light absorption capability of atmospheric BC-containing particles under different pollution levels. Firstly,
14 we analyzed the evolution of BC light absorption capability with increasing air pollution levels and estimated the
15 relationship between the rates of changes in the light absorption capability of BC and in the PM₁ or BC mass concentrations.
16 We then explored the cause of the evolution of light absorption capability of BC with increasing air pollution levels and
17 evaluated the relative importance of regional transport. Finally, we discussed the impact of changes in BC light absorption
18 capability with pollution levels on BC radiative forcing.

19 **2 Methods**

20 **2.1 Sampling site and measurements**

21 The *in-situ* measurements were conducted on the campus of Tsinghua University (Tsinghua site, 40°00'17" N, 116°19'34" E)
22 from November 17-30, 2014. The Tsinghua site (Fig. S1) is located in urban Beijing, China. The megacity Beijing is
23 adjacent to Hebei Province and the megacity Tianjin (Fig. S1), in which considerable industrial manufacturing has led to
24 heavy emissions of air pollution, especially in southern Hebei.

25 Ambient aerosol particles were collected by a PM₁ cyclone and a diffusion silica gel dryer, and they were then analyzed
26 by an aethalometer (AE33, Magee Scientific Corp.), an Aerosol Chemical Speciation Monitor (ACSM, Aerodyne Research
27 Inc.) and a single particle soot photometer (SP2, Droplet Measurement Technologies Inc.). The AE33 can measure the
28 absorption coefficient (σ_{ab}) of sampled aerosols in seven spectral regions (370, 470, 520, 590, 660, 880 and 950 nm). At a
29 wavelength of 880 nm, the absorption of aerosol particles is dominated by BC because the light absorbed by other aerosol
30 components is significantly less (Drinovec et al., 2015; Sandradewi et al., 2008). In this study, the σ_{ab} at 880 nm measured by
31 the AE33 was used to characterize the light absorption of the BC-containing particles. More details on the AE33



1 measurement can be found in the work of Drinovec et al., 2015. Considering the filter-loading effect and multiple-scattering
2 effect (Drinovec et al., 2015; Weingartner et al., 2003; Segura et al., 2014), the aethalometer data was corrected by
3 compensation factors described in the supplementary information (Fig. S2 and the associated discussion). The ACSM and
4 SP2 instruments measured the mass concentrations of non-refractory submicron-scale components (NR-PM₁, i.e., sulfate,
5 nitrate, ammonium, chloride and organics) and refractory BC (rBC), respectively, and the sum of these two measurements
6 was used to estimate the PM₁ mass concentration. The ACSM instrument used in our study was described by Li et al. (2017).

7 The SP2 instrument measures a single BC-containing particle using a 1064 nm Nd:YAG intra-cavity laser beam. As the
8 light-absorbing rBC passes through the laser beam and is heated to its vaporization temperature (~4000 K), it will emit
9 incandescent light (i.e., visible thermal radiation), which is linearly proportional to the mass of the rBC (Moteki and Kondo,
10 2010; Schwarz et al., 2006; Sedlacek et al., 2012). In this study, the calibration curve of rBC mass vs. incandescence signal
11 was obtained from the incandescence signal of size-resolved Aquadag particles (their effective density obtained from Gysel
12 et al., 2011) using a DMA (differential mobility analyzers)-SP2 measurement system. Considering different sensitive of the
13 SP2 to different rBC types (Gysel et al., 2011; Laborde et al., 2012), we corrected SP2 calibration curve by scaling the peak
14 height of incandescence signal for Aquadag particles at each rBC mass based on the relationship between the sensitivity of
15 SP2 to Aquadag and ambient rBC (Laborde et al., 2012). The particle-to-particle mass of ambient rBC can be determined by
16 measuring its incandescence signal and comparing it to the calibration curve. Furthermore, the scattering cross section of a
17 BC-containing particle is obtained from its scattering signal using the leading edge only (LEO)-fit method (Gao et al. 2007).
18 Zhang et al. (2016) has demonstrated the validity of the LEO-fit method for ambient BC-containing particles in China.

19 2.2 SP2 data analysis

20 2.2.1 Aging degree of BC-containing particles

21 Based on the rBC core mass (m_{rBC}) and scattering cross section (C_s) of the BC-containing particle derived from the SP2
22 measurements, the size of the BC-containing particle (D_p), including the BC core and the coating materials, was calculated
23 by Mie theory with a shell-and-core model (Zhang et al., 2016). The D_p is determined by the relationship (1):

$$24 D_p \sim (C_s, D_c, RI_s, RI_c), \quad (1)$$

25 In the relationship (1), the RI_s and RI_c represent the refractive indices of the non-BC shell, respectively. The RI_s value
26 used in this study are 1.50-0i based on values in the literature (Cappa et al., 2012). In term of RI_c , we evaluated the
27 sensitivity of D_p values retrieved by Mie mode to the RI_c values (Fig. S3 and the associated discussion in the supplementary
28 information). In the following calculation, the RI_c of 2.26-1.26i was used (Taylor et al., 2015).

29 The D_c in the relationship (1) is the size of the rBC core and is calculated using the m_{rBC} and rBC core density (ρ_c , 1.8 g
30 cm⁻³ used in this study (Cappa et al., 2012)) assuming a void-free sphere for rBC core, as given in Eq. (2). The size
31 distribution of rBC cores under different pollution levels during the campaign period was displayed in Fig. S4.



$$D_c = \left(\frac{6m_{rBC}}{\pi\rho_c} \right)^{1/3}, \quad (2).$$

As in previous studies (Liu et al., 2013; Sedlacek et al., 2012; Zhang et al., 2016), the aging degree of BC-containing particles was characterized by the D_p/D_c ratio. Higher D_p/D_c ratios for BC-containing particles indicate higher aging degrees, i.e., more coating materials on the BC surface.

In terms of D_p/D_c ratio of BC-containing particles determined by relationship (1) and Eq. (2), we focused on the rBC core size (D_c) above detection limit of SP2 incandescence ($D_c > 75$ nm), while the detection limit of SP2 scattering for the whole particle size (D_p) was not considered in this study. If the BC-containing particles with rBC cores larger than ~75 nm is large enough to be detected by SP2 scattering channel, we would calculate their whole particle size (D_p) using LEO method based on their scattering signal. If not, we would assume that the D_p was equal to the rBC core size (D_c). This assumption might lead to the underestimate of aging degree (D_p/D_c) of the BC-containing particles with size above the incandescence limit and blow the scattering limit. To evaluate the uncertainty of D_p/D_c ratio, we calculated the detect efficiency of SP2 scattering (Fig. S5 in the supplementary information). In terms of BC-containing particles with rBC core larger than 75 nm (SP2 size cut for incandescence) observed in our site during the campaign period, most of them (~90-100%, Fig. S5) exhibited particle size (180-500 nm shown in Fig. R6) larger than SP2 size cut for scattering due to large coating materials on rBC cores. This indicated that the uncertainty of D_p/D_c ratio calculated in this study due to mismatch in the SP2 size cut for incandescence vs scattering is no more than 10%. High detection efficiency of SP2 scattering for BC-containing particles observed in our site can be attribute to their large size (180-500 nm, Fig. S6).

2.2.2 BC optical properties

Based on the size information on BC-containing particles (i.e., D_c and D_p) obtained from the SP2 measurement (discussed in Sec. 2.2.1), we used Mie theory with a shell-and-core model to retrieve the optical properties of BC-containing particles, including the absorption enhancement (E_{ab}) of rBC, mass absorption cross-section (MAC) of BC-containing particles, mass scattering cross section of bare BC core (MSC_{core}) and absorption coefficient (σ_{ab}) of BC-containing particles. The calculation of these parameters is described below.

The E_{ab} characterizes the increase in BC light absorption due to the lens effect of coating materials on the BC surface and is used to quantify the light absorption capability of BC-containing particles in this study. The E_{ab} is determined by the ratio of the absorption cross section of the entire BC-containing particle ($C_{ab,p}$) to that of bare BC core ($C_{ab,c}$), as expressed in Eq. (3):

$$E_{ab} = \frac{C_{ab,p}(D_c, D_p, RI_s, RI_c)}{C_{ab,c}(D_c, RI_c)}, \quad (3)$$

where $C_{ab,p}$ is determined by the D_c , D_p , RI_s and RI_c using Mie calculation, and $C_{ab,c}$ is determined by the D_c and RI_c .

The MAC of BC-containing particles is defined as the $C_{ab,p}$ per unit rBC mass, as Eq. (4):

$$MAC = \frac{C_{ab,p}(D_c, D_p, RI_s, RI_c)}{m_{rBC}}, \quad (4)$$



1 The MSC_{core} is the scattering cross sections of bare BC cores ($C_{sca,c}$) per unit rBC mass, as calculated by Eq. (5):

$$2 \quad MSC_{core} = \frac{C_{sca,c}(D_c, R_{Ic})}{m_{rBC}}. \quad (5)$$

3 The σ_{ab} of BC-containing particles is calculated based on the MAC (Eq. (4)) and the rBC mass concentration (C_{rBC})
4 measured by the SP2, as expressed in Eq. (6). The uncertainties of σ_{ab} of BC-containing particles from Mie calculation was
5 evaluated in the supplementary information (Fig. S7 and the associated discussion).

$$6 \quad \sigma_{ab,calculated} = MAC \times C_{rBC}, \quad (6).$$

7 **2.3 BC effective emission intensity**

8 To evaluate the impact of regional transport on BC-containing particles, we used a variant of the “effective emission
9 intensity” (EEI) defined by Lu et al. (2012) to quantify the amounts of BC over the observation site from different source
10 regions. In this study, the spatial origin of the BC observed at our site was divided into local sources in Beijing and regional
11 sources in other areas (i.e., Hebei, Tianjin, Shanxi and Inner Mongolia, Fig. S1). The EEI takes into account emission,
12 transport, hydrophilic-to-hydrophobic conversion, and removal processes (i.e., dry and wet deposition) of BC throughout the
13 whole atmospheric transport process from the origin of the BC emission to the receptor site. A novel back-trajectory
14 approach was developed by Lu et al. (2012) to calculate EEI values.

15 In this study, the back-trajectory analysis was performed by the Hybrid Single-Particle Lagrangian Integrated Trajectory
16 (HYSPPLIT) model to obtain the transport pathways of BC to the observation site (40°00'17" N, 116°19'34" E) during the
17 campaign period (November 17-30, 2014). The 72-h back-trajectory at 100 m at every hour was calculated with the
18 meteorological fields of NCEP GDAS at a 1°×1° resolution. An anthropogenic BC emission inventory of China in the year
19 2012 at a resolution of 0.25°×0.25° was used to support the back-trajectory analysis. The gridded BC emission data are from
20 the Multi-resolution Emission Inventory for China (MEIC) developed by Tsinghua University (<http://www.meicmodel.org>).

21 We calculated the EEI of BC at a resolution of 0.25°×0.25° based on the algorithm developed by Lu et al. (2012).
22 Following a trajectory l at every hour, the fresh BC particles emitted from a series of spatial grids in sequence (i.e., $l_1, l_2, \dots,$
23 l_i, \dots) are transported to the receptor grid (i.e., l_n). The EEI of trajectory l at the surface grid point i ($EEI_{i,l}$) was determined by
24 Eq. (7):

$$25 \quad EEI_{i,l} = E_i \times TE_{i,l}, \quad (7)$$

26 where E_i is the BC emission at the surface grid point i , and $TE_{i,l}$ represents the BC transport efficiency of trajectory l from
27 the grid point i to the receptor site, as calculated by Eqs. (1)-(4) in Lu et al. (2012).

28 The total EEI of trajectory l characterizes the total amount of BC transported to the observation at every hour, expressed
29 as Eq. (8):

$$30 \quad EEI_{total} = \sum_{i=1}^n EEI_{i,l}, \quad (8).$$

31 **2.4 BC radiative efficiency**



1 In this study, we use a parameter of the simple forcing efficiency (*SFE*) to roughly evaluate the radiative forcing of BC-
2 containing particles. The *SFE* is defined as normalized radiative forcing by BC mass, which is wavelength-dependent (Bond
3 and Bergstrom, 2006; Chen and Bond, 2010; Chylek and Wong, 1995; Saliba et al., 2016). The wavelength-dependent *SFE*
4 for BC-containing particles is determined by Eq. (9):

$$5 \frac{dSFE}{d\lambda} = -\frac{1}{4} \frac{dS(\lambda)}{d\lambda} \tau_{atm}^2(\lambda) (1 - F_c) \times [2(1 - \alpha_s)^2 \beta(\lambda) \cdot MSC_{core}(\lambda) - 4\alpha_s \times MAC(\lambda)], \quad (9)$$

6 in which a wavelength (λ) of 550 nm is used in this study; $dS(\lambda)/d\lambda$ is the spectral solar irradiance, the value of which is
7 from the ASTM G173-03 Reference Spectra ($1.86 \text{ W m}^{-2} \text{ nm}^{-1}$ at 550 nm); and the parameters τ_{atm} , F_c , α_s and β are the
8 atmospheric transmission (0.79), cloud fraction (0.6), urban surface albedo (0.15) and backscatter fraction (0.17),
9 respectively (Jeong et al., 2013; Chen and Bond, 2010; Park et al., 2011; Saliba et al., 2016).

10 **3 Results**

11 **3.1 Light absorption of BC-containing particles during the campaign period**

12 Figure 1 shows the time series of the PM₁ and rBC mass concentration, the diameter of BC-containing particles (D_p) and the
13 light absorption coefficient (σ_{ab}) at 880 nm. During the campaign period, four episodes with different PM₁ evolution
14 processes (Fig. 1a) were observed: November 18-21, November 23-24, November 25-26 and November 28-30. The hourly
15 PM₁ mass concentration ranged from $3.5\text{-}275 \mu\text{g m}^{-3}$, with an average value of $91 \mu\text{g m}^{-3}$ during the observed period. The
16 rBC mass concentration accounted for ~5% of PM₁. The diameter of BC-containing particles (D_p) including rBC cores and
17 coating materials shown in Figure 1(b) exhibited an excellent temporal coherence with the rBC mass concentration. Figure
18 1(b) shows that the number distribution of D_p for BC-containing particles exhibited a peak at 180-320 nm, significantly
19 larger than the peak value (D_c of ~95 nm) for number size distribution of bare rBC cores (Fig. S3a) due to larges of coating
20 materials on BC surface. The size information (namely entire particle size (D_p) and rBC core size (D_c)) of BC-containing
21 particles observed in our study was consistent with that (D_p of ~200-300 nm and D_c of ~70-100 nm) in previous studies in
22 China (Gong et al., 2016; Huang et al., 2012; Wang et al., 2014). Moreover, the D_p exhibited sustained growth from ~180 nm
23 to ~400 nm during a pollution episode, revealing an increase in the amount of coating materials on the BC surface with
24 increasing air pollution levels. With an increase in air pollution, the simultaneous increase in the rBC mass concentration and
25 the amount of coating materials on the BC surface could significantly enhance the light absorption of BC-containing
26 particles. Figure S8 shows that the absorption coefficient at 880 nm for the aerosol particles measured by the AE33 (σ_{ab} ,
27 $\sigma_{ab, measured}$) (dominated by BC component at this wavelength (Drinovec et al., 2015) exhibited an 18-fold increase in conjunction
28 with an increase in the PM₁ concentration from ~10 $\mu\text{g m}^{-3}$ to ~230 $\mu\text{g m}^{-3}$.

29 To valid SP2 measurements and Mie calculation used in this study, we compared the calculated light absorption
30 coefficient ($\sigma_{ab, calculated}$) of BC-containing particles using Eq. (6) with the measured light absorption coefficient ($\sigma_{ab, measured}$)
31 from AE33, as shown in Fig. 1c. The $\sigma_{ab, calculated}$ values for BC-containing particles showed an excellent agreement with the



1 $\sigma_{ab, \text{measured}}$ values measured by the AE33, with a difference of $\sim 10\%$ ($R^2=0.98$). The difference was dominated by the
2 uncertainties from compensation algorithm used in the AE33 measurements ($\sim 10\%$, details shown in Fig. S2 and the
3 associated discussion in the supplementary information) and Mie calculation (smaller than 10% , Fig. S7 and the associated
4 discussion in the supplementary information). The uncertainty evaluation revealed that the difference between $\sigma_{ab, \text{calculated}}$ and
5 $\sigma_{ab, \text{measured}}$ ($\sim 10\%$) shown in Fig. 1c is reasonable. The comparison between the $\sigma_{ab, \text{calculated}}$ and $\sigma_{ab, \text{measured}}$ values implied that
6 the optical properties (i.e., σ_{ab} , MAC and E_{ab}) of the BC-containing particles derived from Mie calculation combining with
7 SP2 measurement data (i.e., rBC concentrations, D_p and D_c) were reliable in our case.

8 **3.2 Enhancement of the light absorption capability of black carbon associated with air pollution**

9 Previous studies reported that the coating materials on the BC surface can significantly enhance the light absorption of BC
10 via the lens effect (Fuller et al., 1999; Jacobson, 2001; Lack and Cappa, 2010; Moffet et al., 2009). In other words, the aging
11 degree of BC-containing particles (i.e., the D_p/D_c ratio) determines their light absorption capability (i.e., the MAC and E_{ab}).
12 However, whether and how the aging degree and light absorption capability of BC-containing particles will change under
13 different pollution levels remains unclear. During the campaign period, we found that the aging degree and light absorption
14 capability of BC-containing particles increased with increasing air pollution levels. Figure 2a shows the D_p/D_c ratio and E_{ab}
15 of BC-containing particles with rBC cores at 75-300 nm under different PM_{10} concentrations in the range of 1.2-3.5 and 1.3-
16 3.1, respectively. In terms of BC-containing particles with a certain rBC core size, their D_p/D_c ratio and E_{ab} were greater
17 under higher PM_{10} concentrations, which could be attributed to more coating materials on BC surface under more pollution
18 environment due to more secondary component formation.

19 As shown in Fig. 2, the enhancement of D_p/D_c ratio and E_{ab} associated with air pollution were size-dependent. Smaller
20 rBC cores exhibited more increase in the aging degree and light absorption capability with pollution development. When
21 PM_{10} concentration increasing from $\sim 10 \mu\text{g m}^{-3}$ to $\sim 230 \mu\text{g m}^{-3}$ during the campaign period, the D_p/D_c ratio and E_{ab} of BC-
22 containing particle with rBC cores at 75-200 nm increased by 26-73% and 13-44%, respectively. The increase of D_p/D_c ratio
23 and E_{ab} associated with air pollution decreased with increasing rBC core size according to an exponential function (Fig.
24 2b). This revealed that the aging degree and light absorption capability for rBC cores smaller than 75 nm (namely lower
25 detection limit of SP2 incandescence) were most likely more than 73% and 44% respectively, and was about $\sim 26\%$ and
26 $\sim 13\%$ for rBC cores larger than 200 nm. The size-dependent increase of D_p/D_c ratio and E_{ab} associated with air pollution
27 indicated that the aging process of smaller rBC was relatively more sensitive to air pollution levels. This could be attributed
28 to the fact that the condensational growth associated with air pollution due to the formation of secondary components is
29 more effective for smaller particles in terms of increasing the diameter (Metcalf et al., 2013).

30 Figure 3 explores the relationship between the change rate of E_{ab} ($k_{E_{ab}}$) and the change rates of PM_{10} and rBC
31 concentrations ($k_{PM_{10}}$ and k_{rBC} , respectively) with pollution development. Linear relationships were estimated, i.e., $k_{E_{ab}} \approx 4.8\%$
32 $k_{PM_{10}}$ and $k_{E_{ab}} \approx 2.5\% k_{rBC}$, revealing that rapid increases in air pollution levels lead to rapid increases in BC light absorption
33 capability. When the PM_{10} concentration exhibited a sharp increase related to an extreme haze episode (Zheng et al., 2015),



1 the increase in BC light absorption capability was dramatic. During the campaign period, k_{Eab} reached a maximum of $7.3\% \text{ h}^{-1}$,
2 accompanied by a k_{PM1} of $107.6\% \text{ h}^{-1}$ and a k_{rBC} of $130.9\% \text{ h}^{-1}$. The growth rate of E_{ab} (for BC samples with $k_{Eab} > 0$: 0.1 -
3 $7.3\% \text{ h}^{-1}$) observed at our study was consistent with the BC aging rate (0.2 - $7.8\% \text{ h}^{-1}$) in previous studies (Cheng et al., 2012;
4 Moteki et al., 2007; Shiraiwa et al., 2007). Moreover, we found that the growth rate of E_{ab} decreased with increasing PM_1
5 mass concentrations (Fig. S9), indicating that the increase in the light absorption capability of BC-containing particles
6 slowed with further pollution development. On average, the growth rate of BC light absorption capability during the
7 campaign period was $\sim 1.2\% \text{ h}^{-1}$. Compared with the values of k_{PM1} and k_{rBC} , the significantly smaller k_{Eab} value indicated that
8 the light absorption capability of BC increased more slowly than the PM_1 or rBC mass concentrations. Smaller growth rate
9 of BC light absorption capability may explain why previous studies (McMeeking et al., 2011; Ram et al., 2009; Wang et al.,
10 2014b; Andreae, et al., 2008) just paid attention to the increase of BC mass concentrations associated with air pollution, but
11 ignored the enhancement of BC light absorption capability. Generally, the light absorption capability (i.e., mass absorption
12 cross-section) of BC was determined by linear regression of the absorption coefficient against BC (or EC) mass
13 concentrations in previous studies (Wang et al., 2014b; Andreae, et al., 2008). Excellently linear relationship between
14 absorption coefficient and BC mass concentrations can be attributed to that the change of absorption coefficient is dominated
15 by increase or decrease of BC mass concentration due to much rapider change of BC mass concentration compared with that
16 of BC light absorption capability. The linear regression method would cover up the fact that the change of the light
17 absorption capability of BC with their mass concentration under different air pollution levels. In our case, if the increase in
18 BC light absorption capability due to increasing BC mass concentration was neglected, the light absorption of BC-containing
19 particles would be underestimated by $\sim 28\%$ under polluted conditions.

20 3.3 Contribution of regional transport

21 BC aging in the atmosphere, a consequence of BC internally mixed with other aerosol components, is associated with
22 atmospheric transport (Gustafsson and Ramanathan, 2016). In Beijing, the rapid increase in aerosol particle concentrations
23 during pollution episodes is most likely caused by regional transport of polluted air mass (Yang et al., 2015; Zheng et al.,
24 2015). Therefore, regional transport of pollution may play an important role in the enhancement of BC light absorption
25 capability associated with air pollution. In this study, we used the EEI analysis (Lu et al., 2012) to explore the effects of
26 regional transport on the increase in BC light absorption capability with increasing pollution levels.

27 Figure 5 shows the spatial distribution ($0.25^\circ \times 0.25^\circ$) of the EEI for BC transported to the observation site under different
28 pollution levels (i.e., clear, slightly polluted and polluted periods) during the campaign period. The spatial origin of the BC
29 observed at our site varied significantly among the different pollution periods. The BC from areas adjacent to Beijing (i.e.,
30 Hebei, Tianjin, Shanxi and Inner Mongolia (Fig. S1), considered as regional sources in this study) accounted for $\sim 21\%$, 39%
31 and $\sim 63\%$ during the clean, slightly polluted and polluted periods, respectively, revealing that the regional contribution to
32 BC over Beijing increased as the air pollution levels increased. Due to the increase of the regional contribution, the total BC



1 transported to the observation site, characterized by the EEI (EEI_{total}) in this study, increased under more polluted condition.
2 Table 1 shows that the EEI_{total} was 4.6 times higher during the polluted period than during the clean period, revealed that
3 regional transport of polluted air mass brought more BC to Beijing. This ~ 4.6 -fold increase in EEI_{total} accounted for 62% of
4 the ~ 7.4 -fold increase in BC mass concentrations from the clean period to the polluted period, suggesting that the BC from
5 adjacent areas with regional transport of polluted air mass increased BC mass concentrations in Beijing, rather than merely
6 adverse local meteorology (e.g., lower planetary boundary layer (PBL) and wind speed).

7 Under different pollution levels, regional transport not only influenced the BC mass concentrations but also the BC aging
8 process and timescale. Table 1 shows that the aging degree (i.e., the D_p/D_c ratio) of BC-containing particles at our site was
9 ~ 2.79 during the polluted period, significantly higher than that observed during the clean period (~ 2.07) and slightly polluted
10 period (~ 2.37). On one hand, under more polluted conditions, more BC-containing particles in Beijing were from regional
11 sources and thus had undergone a longer aging time during the transport than the BC from local sources in Beijing. On the
12 other hand, compared with the BC carried in the clean air mass from the northwest of Beijing during the clean period (Fig.
13 4a), the BC in the polluted air mass undergoing regional transport from the region south of Beijing (i.e., Hebei, one of the
14 most polluted provinces in China) during the polluted period exhibited higher aging rates (Fig. 4c) (Peng et al., 2015). The
15 E_{ab} values of the BC observed at our site were ~ 1.90 , ~ 2.06 and ~ 2.22 during the clean, slightly polluted and polluted
16 periods, respectively (Table 1), showing that the light absorption capability of BC-containing particles observed at our site
17 increased with increasing regional contributions. Our results demonstrated the importance of regional transport in the
18 enhancement of BC light absorption capability associated with air pollution.

19 To further explore the importance of aging during regional transport, its contributions were compared with those of local
20 chemical processes with respect to increases in aging degree and light absorption capability of BC-containing particles
21 associated with air pollution. Considering the formation of coating materials on BC surface is dominated by photochemical
22 oxidation (Metcalf et al., 2013; Peng et al., 2015), we evaluated the contribution of local photochemical production by the
23 changes of O_3 concentrations in the atmosphere. On the other hand, we used the variation of EEI_{total} per hour to evaluate the
24 contributions of aging during regional transport, taking more EEI_{total} more BC from regional transport into account. Figure 5a
25 shows that the EEI_{total} per hour exhibited a temporal coherence with the D_p/D_c ratio and the E_{ab} of BC-containing particles. In
26 contrast, the O_3 concentrations showed a different temporal trend. Therefore, the increases in the aging degree and light
27 absorption capability of BC-containing particles with increasing air pollution were more likely caused by aging during
28 regional transport than by local photochemical production.

29 According to the evolution of the EEI_{total} values and O_3 concentrations with increasing air pollution levels (Fig. 5b1 and
30 Fig.5b2), we separated the pollution levels into two periods. When PM_{10} concentrations were lower than $\sim 120 \mu g m^{-3}$ and
31 rBC mass concentrations were lower than $\sim 6 \mu g m^{-3}$, the normalized EEI_{total} increased from ~ 3 to ~ 18 with increasing air
32 pollution levels, and the O_3 concentrations decreased from ~ 20 ppb to ~ 2 ppb, indicating enhanced regional contributions
33 and weakened local photochemical production at observation site. In this period, Fig. 5b3 and Fig. 5b4 show that the E_{ab} and
34 the D_p/D_c ratio of BC-containing particles increased from ~ 1.9 to ~ 2.2 and from ~ 2.2 to ~ 2.8 , respectively, with the increase



1 in the normalized EEI_{total} (from ~ 3 to 18) and the decrease in the O_3 concentrations (from ~ 20 to 2 ppb). Therefore, in terms
2 of the increase in the BC light absorption capability with increasing air pollution levels, this period (i.e., conditions of
3 $PM_{10} < 120 \mu g m^{-3}$ and $rBC < 6 \mu g m^{-3}$) represented a regional transport-controlled period. The increase in BC light absorption
4 capability (~ 1.9 - 2.2) during this regional transport-controlled period accounted for $\sim 78\%$ of the increase in BC light
5 absorption capability (~ 1.9 - 2.3) with increasing air pollution during the whole campaign period. Therefore, the aging process
6 during the regional transport dominated the increase in the light absorption capability of BC-containing particles in Beijing
7 during the campaign period. Another period is defined by PM_{10} concentrations of more than $\sim 120 \mu g m^{-3}$ and rBC mass
8 concentrations of more than $\sim 6 \mu g m^{-3}$, during which both the EEI_{total} and O_3 concentrations showed slight changes with
9 increasing air pollution levels. In this period, the increase in BC light absorption capability (from ~ 2.2 to ~ 2.3) might be
10 attributed to local heterogeneous chemical production in Beijing.

11 **3.4 Implications for BC radiative forcing**

12 The increase in BC light absorption capability with increasing air pollution levels suggests that greater solar absorption (i.e.,
13 direct radiative forcing (DRF)) by atmospheric BC occurs under more polluted conditions. The DRF of atmospheric BC-
14 containing particles depends not only on the BC mass concentrations but also on the BC forcing efficiency, which strongly
15 depends on the light absorption capability of BC. In this study, the forcing efficiency of BC-containing particles was
16 estimated based on a simple radiation transfer model (Eq. (9)). Figure 6 shows that, the SFE of BC-containing particles at
17 550 nm increased from $\sim 0.8 m^2 g^{-1} nm^{-1}$ to $\sim 1.0 m^2 g^{-1} nm^{-1}$ due to the increase in MAC at 550 nm in the range of ~ 12 - $15 m^2$
18 g^{-1} with increasing pollution levels (i.e., PM_{10} increasing from $\sim 10 \mu g m^{-3}$ to $\sim 230 \mu g m^{-3}$) during the campaign period.
19 Meanwhile, the DRF of BC-containing particles increased from $\sim 0.51 W m^{-2}$ to $\sim 0.63 W m^{-2}$, revealing the importance of
20 BC in terms of solar absorption under more polluted conditions. In this case, the failure to consider the increase in BC light
21 absorption capability with increasing air pollution levels may cause significant underestimation of the radiative forcing of
22 BC-containing particles in Beijing under polluted conditions.

23 The enhanced climate effects of BC aerosols in Beijing could be taken to be representative of polluted regions in China.
24 Previous measurements of BC aerosols in China (Zheng et al., 2015; Wang et al., 2014b; Zhao et al., 2017; Gong et al.,
25 2016; Huang et al., 2013; Andreae et al., 2008; Zhang et al., 2014) showed that the BC mass concentrations in different
26 regions (e.g., Beijing, Xi'an, Nanjing, Shanghai and Guangzhou) reached values of ~ 10 - $50 \mu g m^{-3}$ during polluted periods
27 (Table S1), similar to our measurements. Therefore, our BC aerosol observations in Beijing were not a special case. In
28 China, high concentrations of BC aerosols under polluted conditions always occur on a regional scale due to intense BC
29 emissions (Zhang et al., 2009; Li et al., 2017) and significant regional transport (Zheng et al., 2015; Wang et al., 2014a; Zhao
30 et al., 2013). Our findings in Beijing can provide some implication in the difference of BC radiative forcing in other regions
31 among different air pollution levels.



1 **4 Discussion: breaking the amplification effect by emission control**

2 Our results reveal that under more polluted environment, the BC-containing particles are characterized by more BC mass
3 concentrations and more coating materials on BC surface and therefore higher light absorption capacity. As shown in Fig. 7,
4 this amplification effect on BC light absorption associated with air pollution is caused by increasing BC concentration and at
5 the same time enhanced light absorption capacity of BC-containing particles by speeding up the coating processes in the
6 more polluted air. Variation of both the mass concentration and light absorption capability of BC associated with air
7 pollution strongly depend on the air pollutant emission (e.g., BC, SO₂, NO_x and VOC). Under polluted environment,
8 polluted air mass from high emission areas not only brings more BC, but also accelerates the production of coating materials
9 on BC surface due to more precursors of secondary components.

10 Air pollution control measures may, on the other hand, break this amplification effect by reducing BC concentration and
11 at the same time lowering the light absorption capacity of BC-containing particles by slowing down the coating processes
12 with a cleaner air (Fig. 7). Take air pollution controls during the 2014 Asia-Pacific Economic Cooperation meeting (APEC)
13 in Beijing, China as an example, we found that as a result of emission controls on local Beijing and areas adjacent to Beijing
14 (i.e., Hebei, Tianjin, Shanxi, Henan, Shandong and Inner Mongolia), light absorption of BC-containing particles decreased
15 by significantly during APEC compared to that of before APEC under similar meteorological conditions (Zhang et al., 2018,
16 in prep). This is not only contributed by a reduction of BC mass concentration, but also by lower light absorption capacity of
17 BC-containing particles with less coating materials on BC surface in cleaner atmosphere conditions, indicating that
18 synergetic emission reduction of multi-pollutants could achieve co-benefits of both air quality and climate.

19 **5 Conclusions**

20 The light absorption of BC-containing particles depends not only on the BC mass concentration but also on their light
21 absorption capability (i.e., MAC and E_{ab}). In this work, we investigated the difference of BC light absorption capability
22 under different air pollution conditions. During an intensive field measurement campaign in Beijing, China, we found that
23 with increasing pollution levels, the increase in BC mass concentration was always accompanied by an increase in the light
24 absorption capability of BC, resulting an amplification effect on the light absorption of the ambient BC-containing particles.
25 When PM₁ concentration increased from $\sim 10 \mu\text{g m}^{-3}$ to $\sim 230 \mu\text{g m}^{-3}$ accompanied with the rBC mass concentration in the
26 range of $\sim 0.3\text{-}12 \mu\text{g m}^{-3}$, the BC-containing particles with $\sim 75\text{-}200 \text{ nm}$ rBC cores measured by SP2 techniques showed an
27 increase of 26-73% in the BC aging degree (i.e., the D_p/D_c ratio). According to Mie theory with a shell-and-core model, the
28 26-73% increase in the BC aging degree associated with air pollution could enhance the BC light absorption capability (i.e.,
29 MAC and E_{ab}) by 13-44%. The increase in BC light absorption capability associated with increasing air pollution can be
30 explained by the increase in coating materials on the BC surface under more polluted conditions. Moreover, the increase of
31 the D_p/D_c ratio and E_{ab} with increasing air pollution levels was size-dependent, namely more increase was exhibited for



1 smaller rBC cores. This indicated that the aging degree and light absorption capability of smaller rBC was more sensitive to
2 air pollution levels.

3 During the campaign period, the relationships between the growth rate of the BC light absorption capability ($k_{E_{ab}}$) with
4 air pollution development and that of the PM_{10} and rBC concentrations ($k_{PM_{10}}$ and k_{rBC} , respectively) were estimated: $k_{E_{ab}} \approx$
5 $4.8\% k_{PM_{10}}$, and $k_{E_{ab}} \approx 2.5\% k_{rBC}$. When pollution levels sharply increased with a $k_{PM_{10}}$ of $107.6\% h^{-1}$ and a k_{rBC} of $130.9\% h^{-1}$,
6 the $k_{E_{ab}}$ increased by as much as $7.3\% h^{-1}$. Although the growth rate of the BC light absorption capability was significantly
7 lower than that of the BC mass concentration, the effect of enhanced BC light absorption capability on the light absorption of
8 ambient BC-containing particles under polluted conditions is not negligible. In our case, if we had not considered the
9 increase in the BC light absorption capability with increasing air pollution during the campaign period, the light absorption
10 of BC-containing particles under polluted conditions would have been underestimated by $\sim 28\%$.

11 The increase in BC light absorption capability with increasing pollution levels in Beijing was controlled by aging during
12 regional transport. The EEI analysis showed that $\sim 63\%$ of the BC observed at our site was transported from regional sources
13 (i.e., areas adjacent to Beijing) during the polluted period, whereas the regional contributions were significantly lower
14 ($\sim 21\%$) during the clean period. More BC in more polluted air from regional transport could lead to a higher local BC
15 concentration in Beijing. Not only more BC but also more coatings are carried into Beijing by more polluted regional air
16 mass (Fig. 7 (a)), which can be explained by speeding up coating process (i.e., the production of coating materials on BC
17 surface by photochemistry and heterogeneous chemistry during regional transport) in a more polluted air. Moreover, we
18 separated the change of the aging degree and light absorption capability of BC associated with air pollution into regional
19 transport-controlled region (i.e., $PM_{10} < 120 \mu g m^{-3}$ and $BC < 6 \mu g m^{-3}$) and local chemistry-controlled region (i.e., $PM_{10} >$
20 $120 \mu g m^{-3}$ and $BC > 6 \mu g m^{-3}$). In the regional transport-controlled region, the D_p/D_c and E_{ab} of BC-containing particles in
21 Beijing increased from ~ 2.2 and ~ 1.9 to ~ 2.8 and ~ 2.2 with increasing pollution levels. The further increase of D_p/D_c (~ 2.8
22 to ~ 3.0) and E_{ab} (~ 2.2 to ~ 2.3) associated with air pollution is harder and is mostly likely attributed to local chemical
23 production by heterogeneous chemistry. Therefore, we attributed $\sim 78\%$ of the increase in BC light absorption capability with
24 increasing air pollution during the campaign period to aging during regional transport, demonstrating the regional transport
25 has an important influence on the variations of light absorption capability of BC-containing particles in Beijing under
26 different pollution levels.

27 Due to the increase in BC light absorption capability with increasing air pollution levels, stronger forcing efficiency of
28 the BC-containing particles was found under more polluted conditions. During the campaign period, the BC forcing
29 efficiency increased by $\sim 20\%$ with PM_{10} increasing from $10 \mu g m^{-3}$ to $230 \mu g m^{-3}$, while the DRF values of ambient BC-
30 containing particles increased from $\sim 0.51 W m^{-2}$ to $\sim 0.63 W m^{-2}$. The results identified that BC in more polluted environment
31 exhibited a larger DRF radiative forcing, which was caused not only by the increase of BC mass concentrations but also by
32 the enhancement of BC light absorption capability.

33 The amplification effect on BC DRF due to the increase of BC light absorption capability introduced in this work not
34 only concerns in Beijing but is also likely to operate in other polluted regions in China. The amplification effect not only



1 could increase the direct contribution of BC to air pollution and climate change due to more light absorption, but also would
2 enhance the indirect contribution by stronger aerosol-meteorology and aerosol-climate feedbacks. Our finds in this work can
3 provide some implication in the difference of BC-related effect on air quality and climate under different air pollution
4 conditions (e.g., air clean and polluted environment) due to change in BC light absorption capability associated with air
5 pollution.

6 The air pollution control may break the amplification effect by reducing BC concentration and at the same time lower the
7 light absorption capacity of BC-containing particles by slowdown the coating processes with a cleaner air. Thereby, breaking
8 the amplification effect by emission control would achieve a co-benefit effect by simultaneous mitigation of air pollution and
9 climate change. Further study will focus on if and how emission reduction of BC and other pollutants in China will break the
10 amplification effect.

11 Acknowledgments

12 This work was supported by the National Natural Science Foundation of China (41625020, 41571130032).

13 References

- 14 Andreae, M. O., Schmid, O., Yang, H., Chand, D., Zhen Yu, J., Zeng, L.-M., and Zhang, Y.-H.: Optical properties and
15 chemical composition of the atmospheric aerosol in urban Guangzhou, China, *Atmos. Environ.*, 42, 6335-6350, 2008.
- 16 Bond, T. C., and Bergstrom, R. W.: Light Absorption by Carbonaceous Particles: An Investigative Review, *Aerosol Sci.*
17 *Technol.*, 40, 27-67, 2006.
- 18 Bond, T. C., Habib, G., and Bergstrom, R. W.: Limitations in the enhancement of visible light absorption due to mixing state,
19 *J. Geophys. Res.-Atmos.*, 111, 2006.
- 20 Cappa, C. D., Onasch, T. B., Massoli, P., Worsnop, D. R., Bates, T. S., Cross, E. S., Davidovits, P., Hakala, J., Hayden, K. L.,
21 Jobson, B. T., Kolesar, K. R., Lack, D. A., Lerner, B. M., Li, S.-M., Mellon, D., Nuaaman, I., Olfert, J. S., Petäjä, T., Quinn,
22 P. K., Song, C., Subramanian, R., Williams, E. J., and Zaveri, R. A.: Radiative Absorption Enhancements Due to the Mixing
23 State of Atmospheric Black Carbon, *Science*, 337, 1078-1081, 2012.
- 24 Chen, Y., and Bond, T. C.: Light absorption by organic carbon from wood combustion, *Atmos. Chem. Phys.*, 10, 1773-1787,
25 2010.
- 26 Cheng, Y. F., Eichler, H., Wiedensohler, A., Heintzenberg, J., Zhang, Y. H., Hu, M., Herrmann, H., Zeng, L. M., Liu, S.,
27 Gnauk, T., Brüggemann, E., and He, L. Y.: Mixing state of elemental carbon and non-light-absorbing aerosol components
28 derived from in situ particle optical properties at Xinken in Pearl River Delta of China, *J. Geophys. Res.-Atmos.*, 111, 2006.



- 1 Cheng, Y. F., Heintzenberg, J., Wehner, B., Wu, Z. J., Su, H., Hu, M., and Mao, J. T.: Traffic restrictions in Beijing during the
2 Sino-African Summit 2006: aerosol size distribution and visibility compared to long-term in situ observations, *Atmos. Chem.*
3 *Phys.*, 8, 7583-7594, 2008.
- 4 Cheng, Y. F., Su, H., Rose, D., Gunthe, S. S., Berghof, M., Wehner, B., Achtert, P., Nowak, A., Takegawa, N., Kondo, Y.,
5 Shiraiwa, M., Gong, Y. G., Shao, M., Hu, M., Zhu, T., Zhang, Y. H., Carmichael, G. R., Wiedensohler, A., Andreae, M. O.,
6 and Pöschl, U.: Size-resolved measurement of the mixing state of soot in the megacity Beijing, China: diurnal cycle, aging
7 and parameterization, *Atmos. Chem. Phys.*, 12, 4477-4491, 2012.
- 8 Chylek, P., and Wong, J.: Effect of absorbing aerosols on global radiation budget, *Geophys. Res. Lett.*, 22, 929-931, 1995.
- 9 Drinovec, L., Močnik, G., Zotter, P., Prévôt, A., Ruckstuhl, C., Coz, E., Rupakheti, M., Sciare, J., Müller, T., and
10 Wiedensohler, A.: The "dual-spot" Aethalometer: an improved measurement of aerosol black carbon with real-time loading
11 compensation, *Atmos. Meas. Tech.*, 8, 1965-1979, 2015.
- 12 Fuller, K. A., Malm, W. C., and Kreidenweis, S. M.: Effects of mixing on extinction by carbonaceous particles, *J. Geophys.*
13 *Res.-Atmos.*, 104, 15941-15954, 1999.
- 14 Gao, R. S., Schwarz, J. P., Kelly, K. K., Fahey, D. W., Watts, L. A., Thompson, T. L., Spackman, J. R., Slowik, J. G., Cross,
15 E. S., Han, J. H., Davidovits, P., Onasch, T. B., and Worsnop, D. R.: A Novel Method for Estimating Light-Scattering
16 Properties of Soot Aerosols Using a Modified Single-Particle Soot Photometer, *Aerosol Sci. Technol.*, 41, 125-135, 2007.
- 17 Gong, X., Zhang, C., Chen, H., Nizkorodov, S. A., Chen, J., and Yang, X.: Size distribution and mixing state of black carbon
18 particles during a heavy air pollution episode in Shanghai, *Atmos. Chem. Phys.*, 16, 5399-5411, 2016.
- 19 Gustafsson, Ö., and Ramanathan, V.: Convergence on climate warming by black carbon aerosols, *Proc. Natl. Acad. Sci.*
20 *USA*, 113, 4243-4245, 2016.
- 21 Guo, S., Hu, M., Zamora, M. L., Peng, J., Shang, D., Zheng, J., Du, Z., Wu, Z., Shao, M., Zeng, L., Molina, M. J., and
22 Zhang, R.: Elucidating severe urban haze formation in China, *Proc. Natl. Acad. Sci. USA*, 111, 17373-17378, 2014.
- 23 Gysel, M., Laborde, M., Olfert, J. S., Subramanian, R., and Gröhn, A. J.: Effective density of Aquadag and fullerene soot
24 black carbon reference materials used for SP2 calibration, *Atmos. Meas. Tech.*, 4, 2851-2858, 2011.
- 25 Huang, X.-F., Xue, L., Tian, X.-D., Shao, W.-W., Sun, T.-L., Gong, Z.-H., Ju, W.-W., Jiang, B., Hu, M., and He, L.-Y.:
26 Highly time-resolved carbonaceous aerosol characterization in Yangtze River Delta of China: Composition, mixing state and
27 secondary formation, *Atmos. Environ.*, 64, 200-207, 2013.
- 28 Jacobson, M. Z.: A physically-based treatment of elemental carbon optics: Implications for global direct forcing of aerosols,
29 *Geophys. Res. Lett.*, 27, 217-220, 2000.
- 30 Jacobson, M. Z.: Strong radiative heating due to the mixing state of black carbon in atmospheric aerosols, *Nature*, 409, 695-
31 697, 2001.
- 32 Jeong, C.-H., Herod, D., Dabek-Zlotorzynska, E., Ding, L., McGuire, M. L., and Evans, G.: Identification of the Sources and
33 Geographic Origins of Black Carbon using Factor Analysis at Paired Rural and Urban sites, *Environ. Sci. Technol.*, 47, 8462-
34 8470, 2013.



- 1 Laborde, M., Mertes, P., Zieger, P., Dommen, J., Baltensperger, U., and Gysel, M.: Sensitivity of the Single Particle Soot
2 Photometer to different black carbon types, *Atmos. Meas. Tech.*, 5, 2012.
- 3 Lack, D. A., and Cappa, C. D.: Impact of brown and clear carbon on light absorption enhancement, single scatter albedo and
4 absorption wavelength dependence of black carbon, *Atmos. Chem. Phys.*, 10, 4207-4220, 2010.
- 5 Lesins, G., Chylek, P., and Lohmann, U.: A study of internal and external mixing scenarios and its effect on aerosol optical
6 properties and direct radiative forcing, *J. Geophys. Res.-Atmos.*, 107, 5-12, 2002.
- 7 Li, H., Zhang, Q., Zhang, Q., Chen, C., Wang, L., Wei, Z., Zhou, S., Parworth, C., Zheng, B., Canonaco, F., Prévôt, A. S. H.,
8 Chen, P., Zhang, H., Wallington, T. J., and He, K.: Wintertime aerosol chemistry and haze evolution in an extremely polluted
9 city of the North China Plain: significant contribution from coal and biomass combustion, *Atmos. Chem. Phys.*, 17, 4751-
10 4768, 2017.
- 11 Li, M., Zhang, Q., Kurokawa, J. I., Woo, J. H., He, K., Lu, Z., Ohara, T., Song, Y., Streets, D. G., Carmichael, G. R., Cheng,
12 Y., Hong, C., Huo, H., Jiang, X., Kang, S., Liu, F., Su, H., and Zheng, B.: MIX: a mosaic Asian anthropogenic emission
13 inventory under the international collaboration framework of the MICS-Asia and HTAP, *Atmos. Chem. Phys.*, 17, 935-963,
14 2017.
- 15 Liu, D., Allan, J., Whitehead, J., Young, D., Flynn, M., Coe, H., McFiggans, G., Fleming, Z. L., and Bandy, B.: Ambient
16 black carbon particle hygroscopic properties controlled by mixing state and composition, *Atmos. Chem. Phys.*, 13, 2015-
17 2029, 2013.
- 18 Liu, D., Whitehead, J., Alfarra, M. R., Reyes-Villegas, E., Spracklen, D. V., Reddington, C. L., Kong, S., Williams, P. I.,
19 Ting, Y.-C., Haslett, S., Taylor, J. W., Flynn, M. J., Morgan, W. T., McFiggans, G., Coe, H., and Allan, J. D.: Black-carbon
20 absorption enhancement in the atmosphere determined by particle mixing state, *Nature Geosci.*, 10, 184-188, 2017.
- 21 Liu, S., Aiken, A. C., Gorkowski, K., Dubey, M. K., Cappa, C. D., Williams, L. R., Herndon, S. C., Massoli, P., Fortner, E.
22 C., Chhabra, P. S., Brooks, W. A., Onasch, T. B., Jayne, J. T., Worsnop, D. R., China, S., Sharma, N., Mazzoleni, C., Xu, L.,
23 Ng, N. L., Liu, D., Allan, J. D., Lee, J. D., Fleming, Z. L., Mohr, C., Zotter, P., Szidat, S., and Prévôt, A. S. H.: Enhanced
24 light absorption by mixed source black and brown carbon particles in UK winter, *Nat Commun.*, 6, 8435, 2015.
- 25 Lu, Z., Streets, D. G., Zhang, Q., and Wang, S.: A novel back-trajectory analysis of the origin of black carbon transported to
26 the Himalayas and Tibetan Plateau during 1996–2010, *Geophys. Res. Lett.*, 39, 2012.
- 27 McMeeking, G. R., Morgan, W. T., Flynn, M., Highwood, E. J., Turnbull, K., Haywood, J., and Coe, H.: Black carbon
28 aerosol mixing state, organic aerosols and aerosol optical properties over the United Kingdom, *Atmos. Chem. Phys.*, 11,
29 9037-9052, 2011.
- 30 Menon, S., Hansen, J., Nazarenko, L., and Luo, Y.: Climate Effects of Black Carbon Aerosols in China and India, *Science*,
31 297, 2250-2253, 2002.
- 32 Metcalf, A. R., Loza, C. L., Coggon, M. M., Craven, J. S., Jonsson, H. H., Flagan, R. C., and Seinfeld, J. H.: Secondary
33 Organic Aerosol Coating Formation and Evaporation: Chamber Studies Using Black Carbon Seed Aerosol and the Single-
34 Particle Soot Photometer, *Aerosol Sci. Technol.*, 47, 326-347, 2013.



- 1 Moffet, R. C., and Prather, K. A.: In-situ measurements of the mixing state and optical properties of soot with implications
2 for radiative forcing estimates, *Proc. Natl. Acad. Sci. USA*, 106, 11872-11877, 2009.
- 3 Moteki, N., and Kondo, Y.: Dependence of Laser-Induced Incandescence on Physical Properties of Black Carbon Aerosols:
4 Measurements and Theoretical Interpretation, *Aerosol Sci. Technol.*, 44, 663-675, 2010.
- 5 Moteki, N., Kondo, Y., Miyazaki, Y., Takegawa, N., Komazaki, Y., Kurata, G., Shirai, T., Blake, D. R., Miyakawa, T., and
6 Koike, M.: Evolution of mixing state of black carbon particles: Aircraft measurements over the western Pacific in March
7 2004, *Geophys. Res. Lett.*, 34, 2007.
- 8 Park, S. H., Gong, S. L., Bouchet, V. S., Gong, W., Makar, P. A., Moran, M. D., Stroud, C. A., and Zhang, J.: Effects of black
9 carbon aging on air quality predictions and direct radiative forcing estimation, *Tellus B*, 63, 1026-1039, 2011.
- 10 Peng, J., Hu, M., Guo, S., Du, Z., Zheng, J., Shang, D., Levy Zamora, M., Zeng, L., Shao, M., Wu, Y.-S., Zheng, J., Wang,
11 Y., Glen, C. R., Collins, D. R., Molina, M. J., and Zhang, R.: Markedly enhanced absorption and direct radiative forcing of
12 black carbon under polluted urban environments, *Proc. Natl. Acad. Sci. USA*, 113, 4266-4271, 2016.
- 13 Ram, K., and Sarin, M. M.: Absorption Coefficient and Site-Specific Mass Absorption Efficiency of Elemental Carbon in
14 Aerosols over Urban, Rural, and High-Altitude Sites in India, *Environ. Sci. Technol.*, 43, 8233-8239, 2009.
- 15 Ramanathan, V., and Carmichael, G.: Global and regional climate changes due to black carbon, *Nature Geosci.*, 1, 221-227,
16 2008.
- 17 Saliba, G., Subramanian, R., Saleh, R., Ahern, A. T., Lipsky, E. M., Tasoglou, A., Sullivan, R. C., Bhandari, J., Mazzoleni,
18 C., and Robinson, A. L.: Optical properties of black carbon in cookstove emissions coated with secondary organic aerosols:
19 Measurements and modeling, *Aerosol Sci. Technol.*, 50, 1264-1276, 2016.
- 20 Sandradewi, J., Prévôt, A. S., Szidat, S., Perron, N., Alfarra, M. R., Lanz, V. A., Weingartner, E., and Baltensperger, U.:
21 Using aerosol light absorption measurements for the quantitative determination of wood burning and traffic emission
22 contributions to particulate matter, *Environ. Sci. Technol.*, 42, 3316-3323, 2008.
- 23 Schnaiter, M., Linke, C., Möhler, O., Naumann, K. H., Saathoff, H., Wagner, R., Schurath, U., and Wehner, B.: Absorption
24 amplification of black carbon internally mixed with secondary organic aerosol, *J. Geophys. Res.-Atmos.*, 110, 2005.
- 25 Schwarz, J. P., Gao, R. S., Fahey, D. W., Thomson, D. S., Watts, L. A., Wilson, J. C., Reeves, J. M., Darbeheshti, M.,
26 Baumgardner, D. G., Kok, G. L., Chung, S. H., Schulz, M., Hendricks, J., Lauer, A., Kärcher, B., Slowik, J. G., Rosenlof, K.
27 H., Thompson, T. L., Langford, A. O., Loewenstein, M., and Aikin, K. C.: Single-particle measurements of midlatitude black
28 carbon and light-scattering aerosols from the boundary layer to the lower stratosphere, *J. Geophys. Res.-Atmos.*, 111, 2006.
- 29 Sedlacek, A. J., Lewis, E. R., Kleinman, L., Xu, J., and Zhang, Q.: Determination of and evidence for non-core-shell
30 structure of particles containing black carbon using the Single-Particle Soot Photometer (SP2), *Geophys. Res. Lett.*, 39, 2012.
- 31 Segura, S., Estellés, V., Titos, G., Lyamani, H., Utrillas, M. P., Zotter, P., Prévôt, A. S. H., Močnik, G., A lados-Arboledas,
32 L., and Martínez-Lozano, J. A.: Determination and analysis of in situ spectral aerosol optical properties by a multi-
33 instrumental approach, *Atmos. Meas. Tech.*, 7, 2373-2387, 2014.



- 1 Shiraiwa, M., Kondo, Y., Iwamoto, T., and Kita, K.: Amplification of Light Absorption of Black Carbon by Organic Coating,
2 *Aerosol Sci. Technol.*, 44, 46-54, 2010.
- 3 Shiraiwa, M., Kondo, Y., Moteki, N., Takegawa, N., Miyazaki, Y., and Blake, D. R.: Evolution of mixing state of black
4 carbon in polluted air from Tokyo, *Geophys. Res. Lett.*, 34, 2007.
- 5 Sun, Y., Jiang, Q., Wang, Z., Fu, P., Li, J., Yang, T., and Yin, Y.: Investigation of the sources and evolution processes of
6 severe haze pollution in Beijing in January 2013, *J. Geophys. Res.-Atmos.*, 119, 4380-4398, 2014.
- 7 Taylor, J. W., Allan, J. D., Liu, D., Flynn, M., Weber, R., Zhang, X., Lefer, B. L., Grossberg, N., Flynn, J., and Coe, H.:
8 Assessment of the sensitivity of core / shell parameters derived using the single-particle soot photometer to density and
9 refractive index, *Atmos. Meas. Tech.*, 8, 1701-1718, 2015.
- 10 Wang, L. T., Wei, Z., Yang, J., Zhang, Y., Zhang, F. F., Su, J., Meng, C. C., and Zhang, Q.: The 2013 severe haze over
11 southern Hebei, China: model evaluation, source apportionment, and policy implications, *Atmos. Chem. Phys.*, 14, 3151-
12 3173, 2014a.
- 13 Wang, Q., Huang, R. J., Cao, J., Han, Y., Wang, G., Li, G., Wang, Y., Dai, W., Zhang, R., and Zhou, Y.: Mixing State of
14 Black Carbon Aerosol in a Heavily Polluted Urban Area of China: Implications for Light Absorption Enhancement, *Aerosol
15 Sci. Technol.*, 48, 689-697, 2014b.
- 16 Weingartner, E., Saathoff, H., Schnaiter, M., Streit, N., Bitnar, B., and Baltensperger, U.: Absorption of light by soot
17 particles: determination of the absorption coefficient by means of aethalometers, *J. Aerosol Sci.*, 34, 1445-1463, 2003
- 18 Yang, Y. R., Liu, X. G., Qu, Y., An, J. L., Jiang, R., Zhang, Y. H., Sun, Y. L., Wu, Z. J., Zhang, F., Xu, W. Q., and Ma, Q. X.:
19 Characteristics and formation mechanism of continuous hazes in China: a case study during the autumn of 2014 in the North
20 China Plain, *Atmos. Chem. Phys.*, 15, 8165-8178, 2015.
- 21 Zhang, G., Bi, X., He, J., Chen, D., Chan, L. Y., Xie, G., Wang, X., Sheng, G., Fu, J., and Zhou, Z.: Variation of secondary
22 coatings associated with elemental carbon by single particle analysis, *Atmos. Environ.*, 92, 162-170, 2014.
- 23 Zhang, Q., Streets, D. G., Carmichael, G. R., He, K. B., Huo, H., Kannari, A., Klimont, Z., Park, I. S., Reddy, S., Fu, J. S.,
24 Chen, D., Duan, L., Lei, Y., Wang, L. T., and Yao, Z. L.: Asian emissions in 2006 for the NASA INTEX-B mission, *Atmos.
25 Chem. Phys.*, 9, 5131-5153, 2009.
- 26 Zhang, R., Khalizov, A. F., Pagels, J., Zhang, D., Xue, H., and McMurry, P. H.: Variability in morphology, hygroscopicity,
27 and optical properties of soot aerosols during atmospheric processing, *Proc. Natl. Acad. Sci. USA*, 105, 10291-10296, 2008.
- 28 Zhang, Y., Zhang, Q., Cheng, Y., Su, H., Kecorius, S., Wang, Z., Wu, Z., Hu, M., Zhu, T., Wiedensohler, A., and He, K.:
29 Measuring the morphology and density of internally mixed black carbon with SP2 and VTDMA: new insight into the
30 absorption enhancement of black carbon in the atmosphere, *Atmos. Meas. Tech.*, 9, 1833-1843, 2016.
- 31 Zhao, Q., Shen, G., Li, L., Chen, F., Qiao, Y., Li, C., Liu, Q., and Han, J.: Ambient Particles (PM₁₀, PM_{2.5} and PM_{1.0}) and
32 PM_{2.5} Chemical Components in Western Yangtze River Delta (YRD): An Overview of Data from 1-year On line Continuous
33 Monitoring at Nanjing, *Aerosol Sci. Eng.*, 2017.



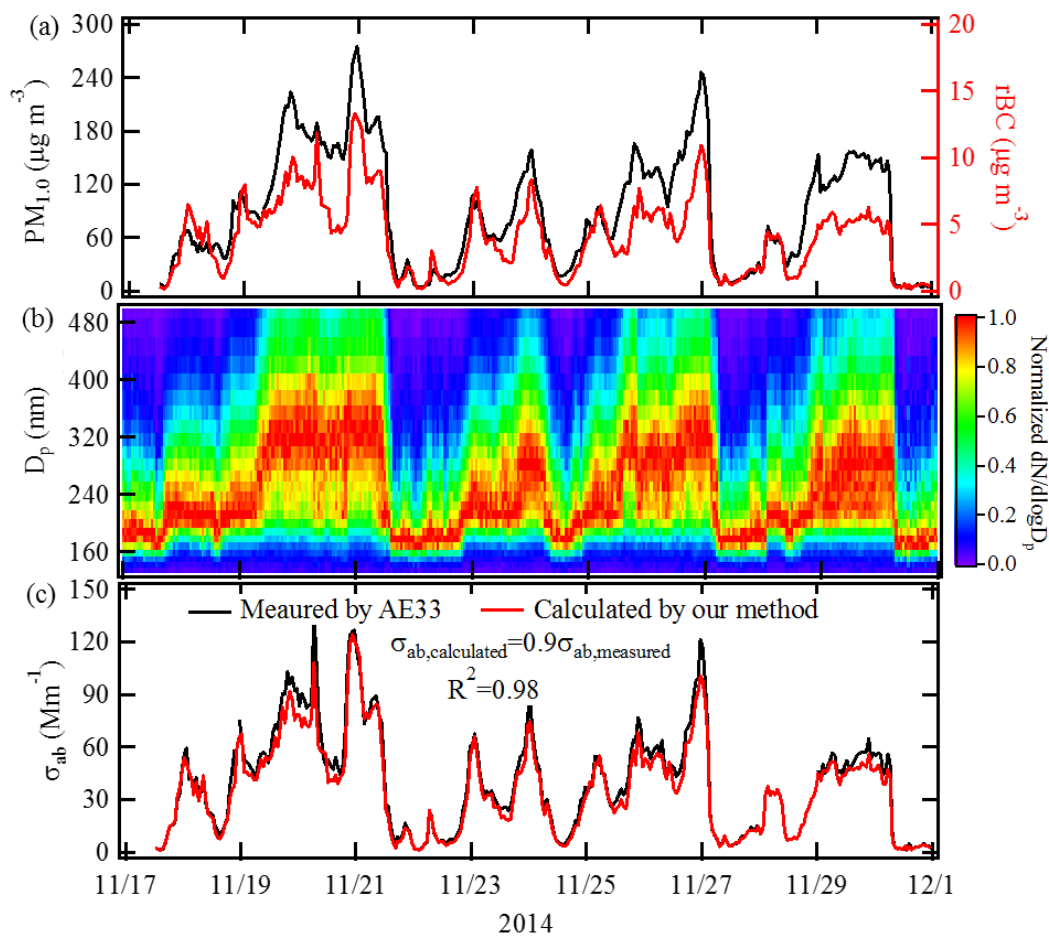
- 1 Zhao, X. J., Zhao, P. S., Xu, J., Meng, W., Pu, W. W., Dong, F., He, D., and Shi, Q. F.: Analysis of a winter regional haze
2 event and its formation mechanism in the North China Plain, *Atmos. Chem. Phys.*, 13, 5685-5696, 2013.
- 3 Zheng, G., Duan, F., Ma, Y., Zhang, Q., Huang, T., Kimoto, T., Cheng, Y., Su, H., and He, K.: Episode-Based Evolution
4 Pattern Analysis of Haze Pollution: Method Development and Results from Beijing, China, *Environ. Sci. Technol.*, 50, 4632-
5 4641, 2016.
- 6 Zheng, G. J., Duan, F. K., Su, H., Ma, Y. L., Cheng, Y., Zheng, B., Zhang, Q., Huang, T., Kimoto, T., Chang, D., Pöschl, U.,
7 Cheng, Y. F., and He, K. B.: Exploring the severe winter haze in Beijing: the impact of synoptic weather, regional transport
8 and heterogeneous reactions, *Atmos. Chem. Phys.*, 15, 2969-2983, 2015.



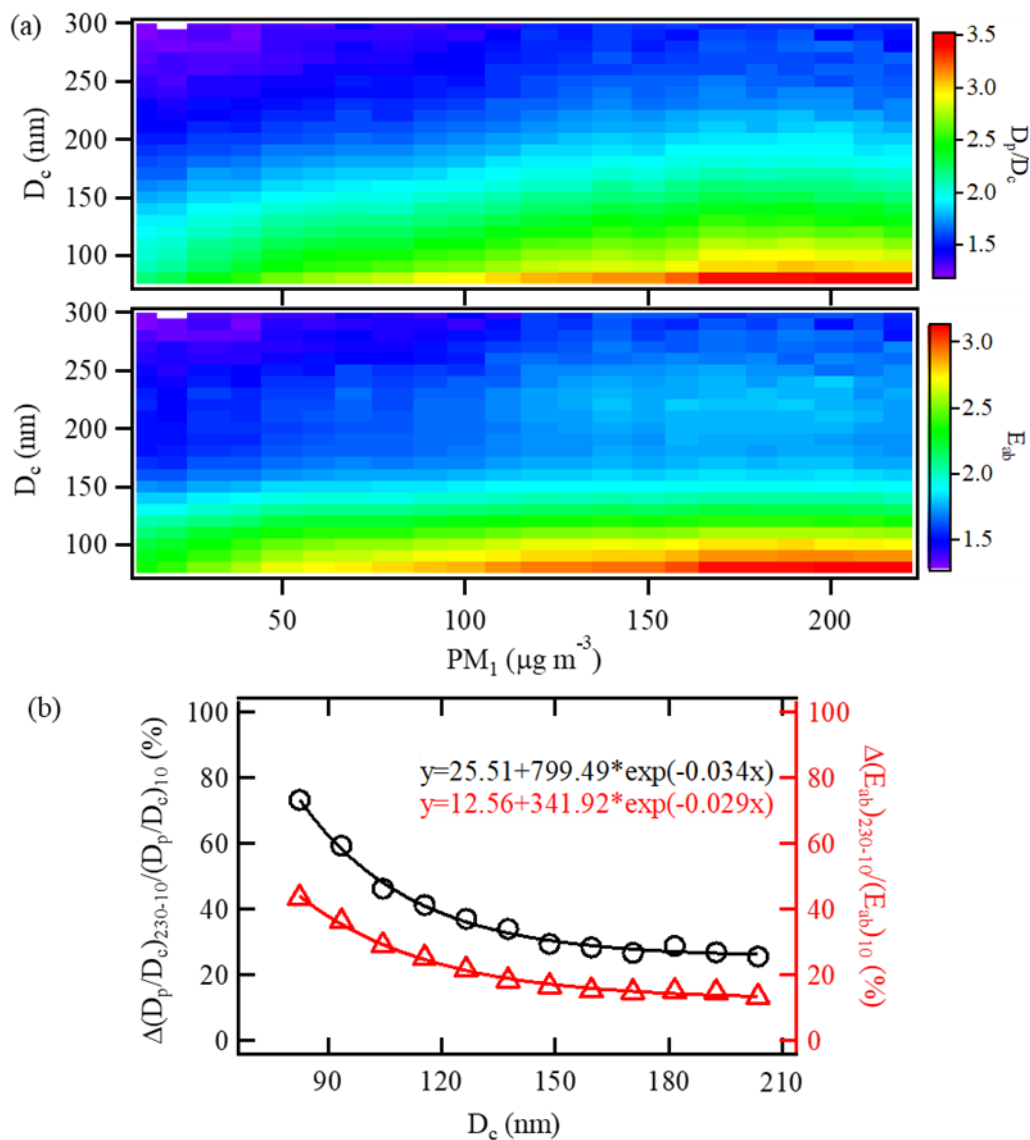
1 **Table 1.** The average PM_{10} mass concentration, rBC mass concentration, normalized EEI_{total} , $EEI_{adjacent}/EEI_{total}$ ratio, D_p/D_c
2 ratio and E_{ab} during clean, slightly polluted and polluted periods. $EEI_{adjacent}$ is the EEI of BC from areas adjacent to Beijing;
3 the $EEI_{adjacent}/EEI_{total}$ ratio reflects the amount of BC contributed by regional transport to the total amount of BC observed at
4 our site. The clean ($PM_{2.5} \leq 35 \mu g m^{-3}$), slightly polluted ($35 \mu g m^{-3} < PM_{2.5} \leq 115 \mu g m^{-3}$) and polluted ($PM_{2.5} > 115 \mu g m^{-3}$)
5 periods were classified according to the Air Quality Index (Zheng et al. 2015).

	Clean	Slightly polluted	Polluted
PM_{10} ($\mu g cm^{-3}$)	12.57	54.26	141.93
rBC ($\mu g cm^{-3}$)	0.82	2.89	6.07
Normalized EEI_{total}	3.68	9.19	16.87
$EEI_{adjacent}/EEI_{total}$	0.21	0.39	0.63
D_p/D_c	2.07	2.37	2.79
E_{ab}	1.90	2.06	2.22

6

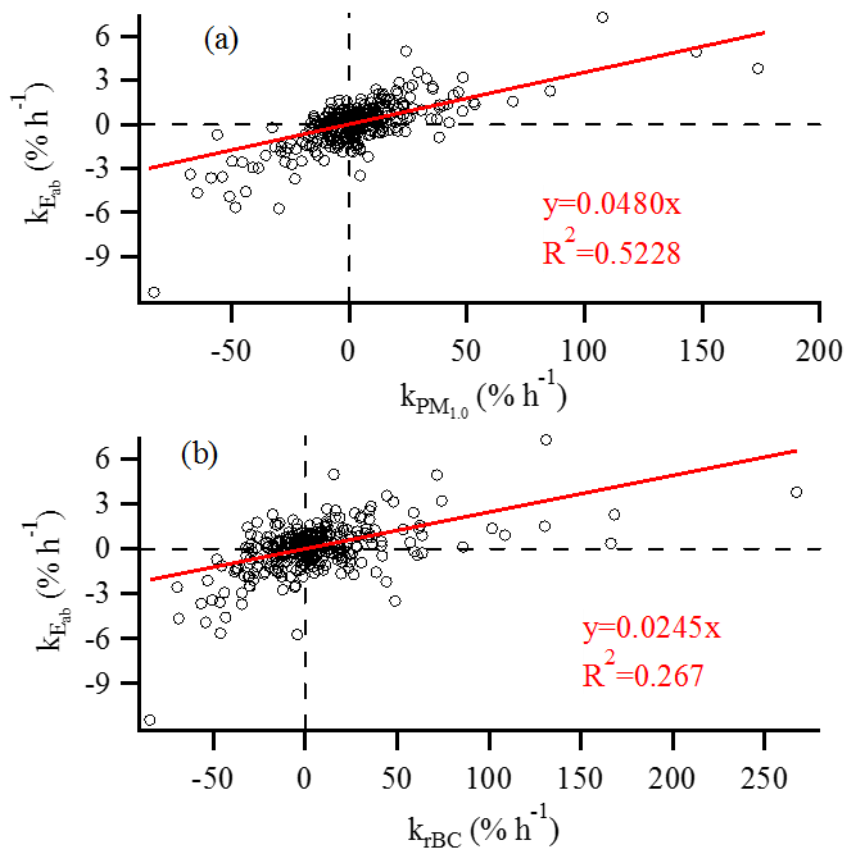


1
2 **Figure 1.** Time series of (a) the PM₁ and rBC mass concentrations, (b) the diameter of BC-containing particles (D_p) and (c)
3 the light absorption coefficient (σ_{ab}) at 880 nm. The correlation between the calculated σ_{ab} ($\sigma_{ab, \text{calculated}}$) using Mie theory
4 combined with SP2 measurements and the measured σ_{ab} ($\sigma_{ab, \text{measured}}$) by the AE33 is also shown in (c).



1
 2 **Figure 2.** (a) The aging degree (D_p/D_c ratio) and light absorption capability (E_{ab}) of BC-containing particles with size-resolved rBC cores
 3 (D_c) under different PM_{10} concentration; (b) the increase ratio of the D_p/D_c and E_{ab} of BC-containing particles with PM_{10} concentration
 4 increasing from $10 \mu g m^{-3}$ to $230 \mu g m^{-3}$ ($\Delta(D_p/D_c)_{230-10}/(D_p/D_c)_{10}$ and $\Delta(E_{ab})_{230-10}/(E_{ab})_{10}$) as a function of rBC core size (D_c). The
 5 $\Delta(D_p/D_c)_{230-10}$ or $\Delta(E_{ab})_{230-10}$ value is the difference between D_p/D_c ratio or E_{ab} with PM_{10} concentration of $230 \mu g m^{-3}$ ($(D_p/D_c)_{230}$ or
 6 $(E_{ab})_{230}$) and that with PM_{10} concentration of $10 \mu g m^{-3}$ ($(D_p/D_c)_{10}$ or $(E_{ab})_{10}$).

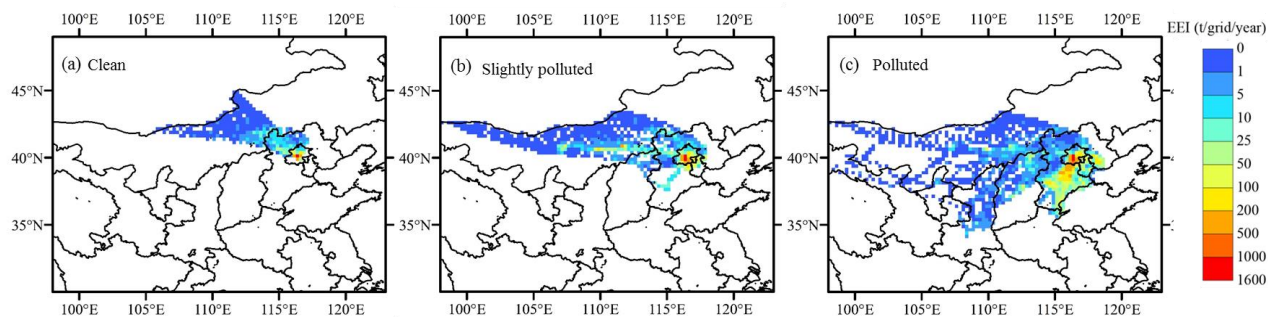
7



1

2 **Figure 3.** Correlation between the growth rate of E_{ab} ($k_{E_{ab}}$) and the growth rates of PM_1 and rBC mass concentrations (k_{PM_1}

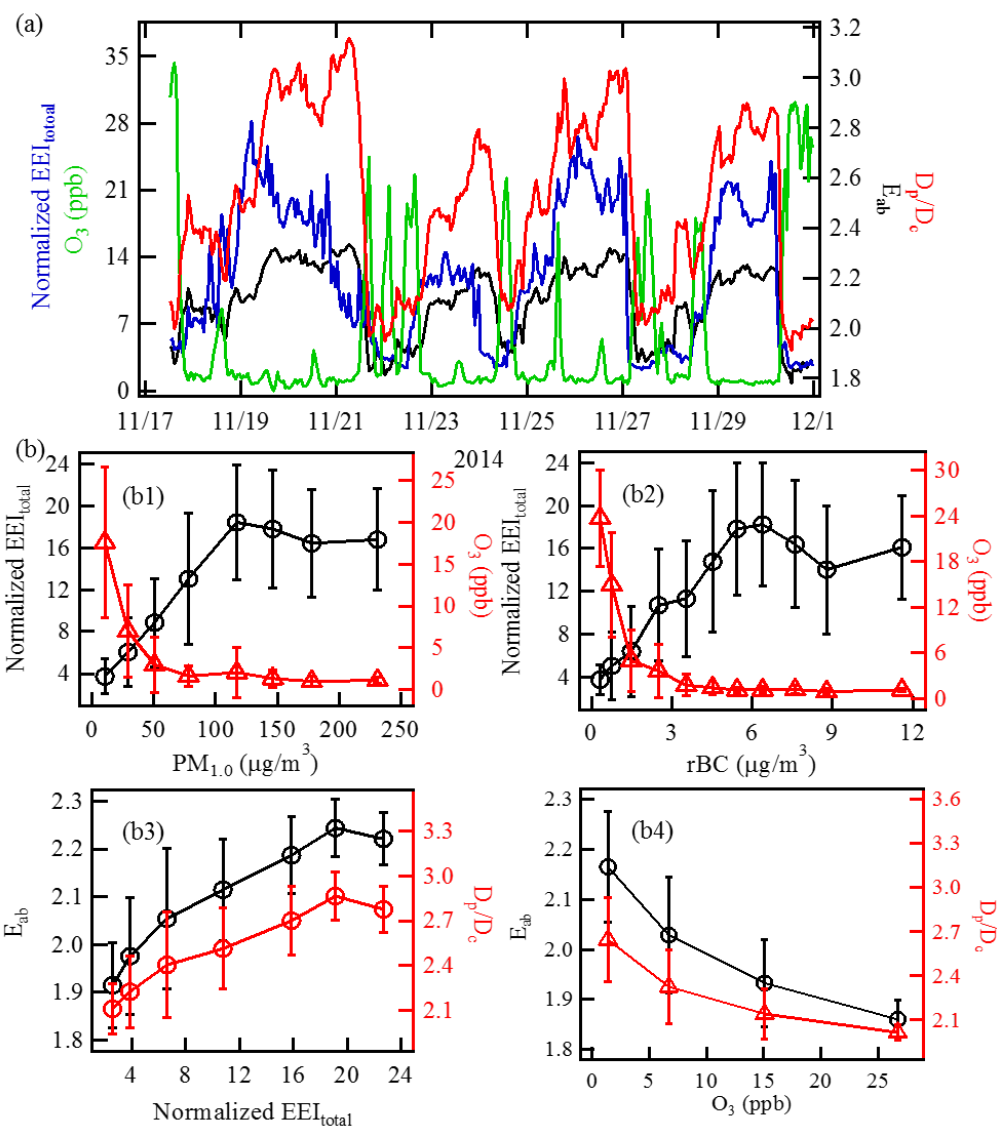
3 and k_{rBC} , respectively) during the campaign period.



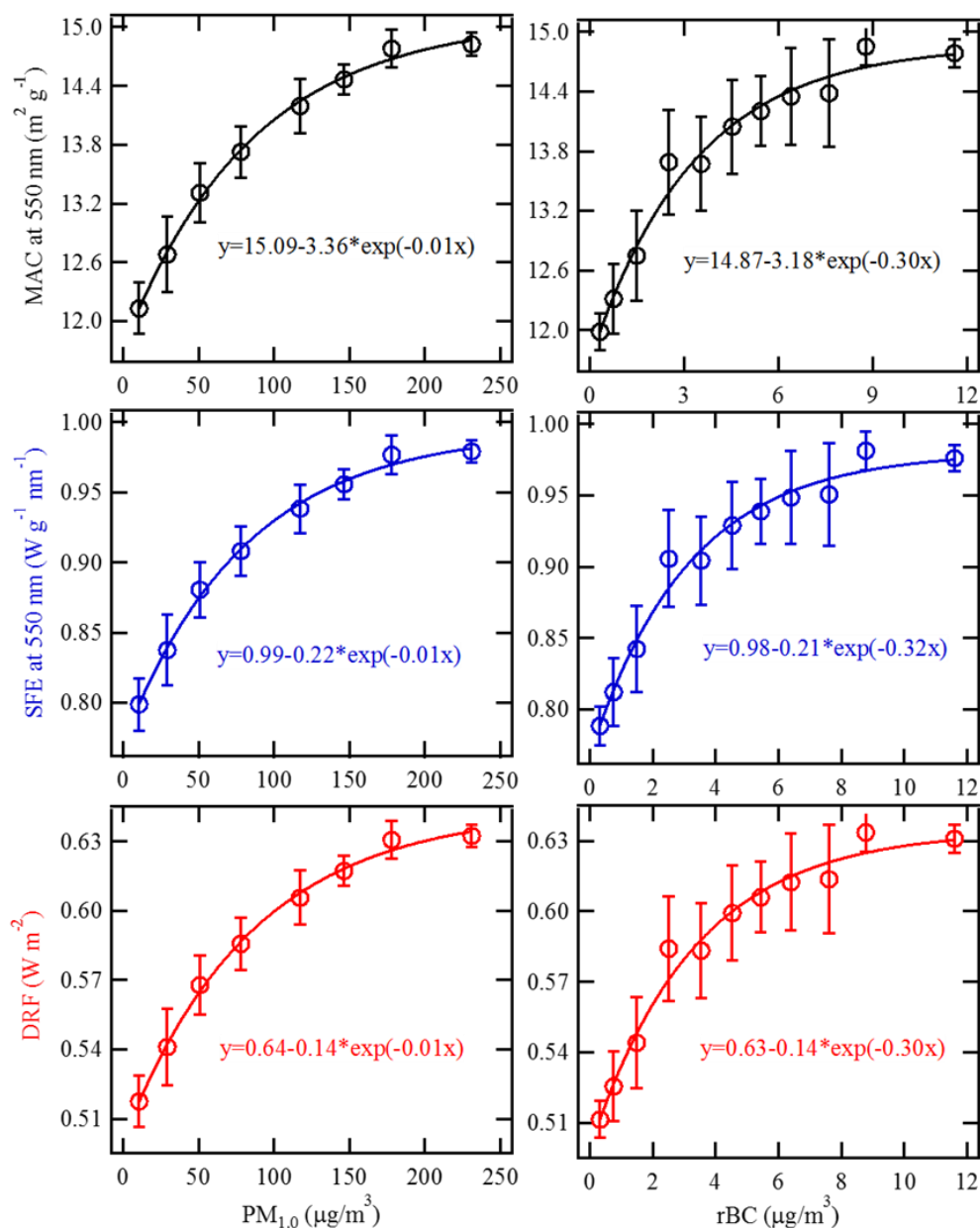
1

2

3 **Figure 4.** Spatial distribution ($0.25 \times 0.25^\circ$) of the effective emission intensity (EEI) for BC transported to the observation
 4 site ($40^\circ 00' 17''$ N, $116^\circ 19' 34''$ E) during clean, slightly polluted and polluted periods. The clean ($PM_{2.5} \leq 35 \mu\text{g m}^{-3}$), slightly
 5 polluted ($35 \mu\text{g m}^{-3} < PM_{2.5} \leq 115 \mu\text{g m}^{-3}$) and polluted ($PM_{2.5} > 115 \mu\text{g m}^{-3}$) periods were classified according to the Air
 6 Quality Index (Zheng et al. 2015).

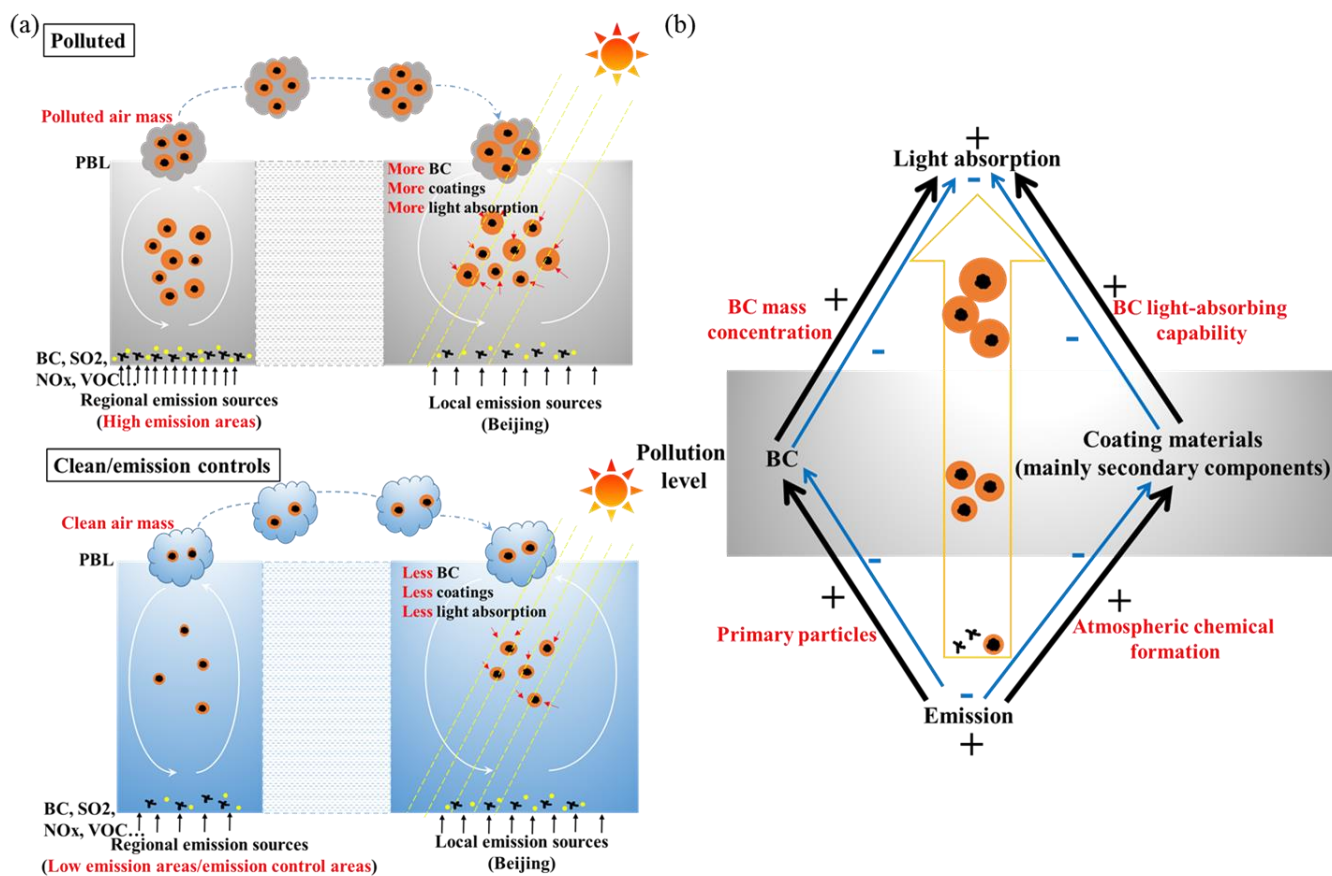


1
 2 **Figure 5.** (a) Time series of the normalized EEI_{total} , D_p/D_c ratios and E_{ab} of BC-containing particles and the O_3
 3 concentration during the campaign period. (b) Variations in the D_p/D_c and E_{ab} of BC-containing particles with the
 4 normalized EEI_{total} and O_3 concentration.



1

2 **Figure 6.** Variations in the *MAC*, *SFE* and *DRF* of BC-containing particles with the PM_{10} and rBC mass concentrations. The
3 *DRF* values for BC-containing particles at different pollution levels were obtained by scaling the average *DRF* (0.32 W m^{-2})
4 of externally mixed BC with an average *MAC* of $7.5 \text{ m}^2 \text{ g}^{-1}$ from various climate models (Bond et al., 2013).



1
 2 **Figure 7.** Conceptual scheme of amplification effect on BC light absorption associated with air pollution.